Inorg. Chem. **2007**, *46*, 6283–6290

Amine-Controlled Assembly of Metal–Sulfite Architecture from 1D Chains to 3D Framework

Cristina Austria,[†] Jian Zhang,[†] Henry Valle,[†] Qichun Zhang,[§] Emily Chew,[†] Dan-Tam Nguyen,[†] J. Y. Gu,[‡] Pingyun Feng,[§] and Xianhui Bu*,[†]

Department of Chemistry and Biochemistry, Department of Physics and Astronomy, California State University, Long Beach, 1250 Bellflower Boulevard, Long Beach, California 90840, and Department of Chemistry, University of California, Riverside, California 92521

Received February 19, 2007

Whereas open-framework materials have been made in a variety of chemical compositions, few are known in which 3-connected SO_3^{2-} anions serve as basic building units. Here, we report four new metal–sulfite polymeric structures, $(ZnSO_3)$Py (**1**, py = pyridine), $(ZnSO_3)_2$(2,2′-bipy)H_2O (**2**, 2,2′-bipy = 2,2′-bipyridine), $(ZnSO_3)_2$(TMDPy) (**3**, TMDPy = 4,4′-trimethylenedipyridine), and $(MnSO_3)_2$en (**4**, en = ethylenediamine) that have been synthesized hydrothermally and structurally characterized. In these compounds, low-dimensional 1D and 2D inorganic subunits are assembled into higher 2D or 3D covalent frameworks by organic ligands. In addition to the structure-directing effect of organic ligands, the flexible coordination chemistry of Zn^{2+} and SO_3^{2-} also contributes to the observed structural diversity. In compounds **1**–**3**, Zn^{2+} sites alternate with trigonal pyramidal SO_3^{2-} anions to form three types of $[ZnSO_3]_n$ chains, whereas in compound **4**, a 2D-corrugated $[MnSO_3]_n$ layer is present. Compound **1** features a rail-like chain with pendant pyridine rings. The π–π interaction between 2,2′-bipy ligands is found between adjacent chains in compound **2**, resulting in 2D sheets that are further stacked through interlayer hydrogen bonds. Compound **3** exhibits a very interesting inorganic $[(ZnSO_3)_2]_n$ chain constructed from two chairlike subunits, and such chains are bridged by TMDPy ligands into a 2D sheet. In compound **4**, side-by-side helical chains permeate through 2D-corrugated $[MnSO_3]_n$ layers, which are pillared by neutral ethylenediamine molecules into a 3D framework that can be topologically represented as a (3,6)-connected net. The results presented here illustrate the rich structural chemistry of metal–sulfites and the potential of sulfite anions as a unique structural building block for the construction of novel open-framework materials, in particular, those containing polymeric inorganic subunits that may have interesting physical properties such as low-dimensional magnetism or electronic properties.

Introduction

Open-framework and porous solids have found widespread applications as catalysts, adsorbents, ion-exchangers, and so forth.[1] These important materials have been made in a variety of compositions, such as silicates, phosphates, germanates, borates, phosphites, and sulfides.[2–4] Recently, there has been an increasing interest in the use of 3-connected centers as basic structural units for the construction of open-framework materials.[5–8] The presence of 3-connected centers has been

* To whom correspondence should be addressed. E-mail: xbu@csulb.edu.
[†] Department of Chemistry and Biochemistry, California State University, Long Beach.
[‡] Department of Physics and Astronomy, California State University, Long Beach.
[§] Department of Chemistry, University of California, Riverside.

(1) (a) Breck, D. W. *Zeolite Molecular Sieves*; Wiley & Sons: New York, 1974. (b) Flanigen, E. M. In *Introduction to Zeolite Science and Practice*; van Bekkum, H.; Flanigen, E. M.; Jansen, J. C., Eds.; Elsevier Science: New York, 1991; pp 13−34. (c) Wilson, S. T.; Lok, B. M.; Messina, C. A.; Cannan, T. R.; Flanigen, E. M. *J. Am. Chem. Soc.* **1982**, *104*, 1146−1147. (d) Yaghi, O. M.; O'Keeffe, M.; Ockwig, N. W.; Chae, H. K.; Eddaoudi, M.; Kim, J. *Nature* **2003**, *423*, 705−714. (e) Palmqvist, A. E. C.; Iversen, B. B.; Zanghellini, E.; Behm, M.; Stucky, G. D. *Angew. Chem. Int. Ed.* **2004**, *43*, 700−704.

(2) (a) Cheetham, A. K.; Ferey, G.; Loiseau, T. *Angew. Chem. Int. Ed.* **1999**, *38*, 3268. (b) Zou, X.; Conradsson,; Klingstedt, M.; Dadachov, M. S.; O'Keeffe, M. *Nature* **2005**, *437*, 716−719.

(3) (a) Liao, Y.-C.; Jiang, Y.-C.; Wang, S.-L. *J. Am. Chem. Soc.* **2005**, *127*, 12794−12795. (b) Tang, M.-F.; Lii, K.-H. *J. Solid State Chem.* **2004**, *177*, 1912−1918.

(4) (a) Feng, P.; Bu, X.; Stucky, G. D. *Nature* **1997**, *388*, 735−741. (b) Bu, X.; Feng, P.; Stucky, G. D. *Science* **1997**, *278*, 2080−2085.

(5) Fan, J.; Slebodnick, C.; Troya, D.; Angel, R.; Hanson, B. E. *Inorg. Chem.* **2005**, *44*, 2719−2727.

(6) (a) Johnstone, J. A.; Harrison, W. T. A. *Inorg. Chem.* **2004**, *43*, 4567−4569. (b) Gordon, L. E.; Harrison, W. T. A. *Inorg. Chem.* **2004**, *43*, 1808−1809. (c) Harrison, W. T. A. *Curr. Opin. Solid State Mater. Sci.* **2002**, *6*, 407−413.

10.1021/ic070325h CCC: $37.00
Published on Web 07/10/2007

recognized to lead to large pore sizes and low framework density (e.g., −CLO, JDF-20), both of which are desirable features in porous materials.[9]

There exist a number of different 3-connected building blocks, both organic and inorganic. Among inorganic units, oxoanions are the most common. Such oxoanions include planar BO_3^{3-} and CO_3^{2-} and pyramidal SnO_3^{4-}, SO_3^{2-}, SeO_3^{2-}, and HPO_3^{2-}.[10−12] Among these 3-connected units, phosphites are particularly useful for creating open-framework solids. In comparison, little is known about open-framework sulfites.[13] The work reported here is part of our systematic exploration of open-framework materials containing 3-connected building units such as phosphites and sulfites.[14−15] It deals with a compositional domain (i.e., inorganic−organic hybrid metal−sulfites) about which very little crystal chemistry is known.

Here, we report four new metal−sulfite polymeric structures, $(ZnSO_3)$Py (**1**, py = pyridine), $(ZnSO_3)_2$(2,2′-bipy)-H_2O (**2**, 2,2′-bipy = 2,2′-bipyridine), $(ZnSO_3)_2$(TMDPy) (**3**, TMDPy = 4,4′-trimethylenedipyridine), and $(MnSO_3)_2$en (**4**, en = ethylenediamine) that have been synthesized hydrothermally and structurally characterized. This work represents an early step toward the exploration of the inorganic−organic hybrid system based on metal−sulfites. Unlike many metal−organic framework structures in which isolated organic and inorganic units (0D) are joined into higher-dimensional frameworks (1D to 3D), these metal−sulfite materials have a strong tendency to form polymeric inorganic subunits that are subsequently joined into higher-dimensional structures through bifunctional organic ligands. The existence of polymeric inorganic subunits opens the door for the integration of useful physical properties (e.g., low-dimensional magnetism, electronic conductivity) into these materials. In the materials reported here, 1D and 2D inorganic subunits are assembled into 2D and 3D covalent frameworks. The rich crystal chemistry is a result of the unique structural directing effect of organic ligands, coupled with variable coordination chemistry of Zn^{2+} (or Mn^{2+}) and SO_3^{2-} building units.

Experimental Section

Synthesis. $(ZnSO_3)$Py (1). Zinc nitrate hexahydrate (98%, 0.3050 g), ammonium sulfite monohydrate (92%, 0.4028 g), pyridine (0.2058 g), and distilled water (3.990 g) were mixed in a 15 mL glass vial, and the mixture was stirred for 20 min. The pH of the mixture was 7.10. The vial was then sealed and heated at 110 °C for 5 d. The vial was subsequently allowed to cool to room temperature. The colorless crystals were obtained in 65% yield. Results of elemental analysis (in wt %) for **1**, $C_5H_5NO_3SZn$, are 26.29 (calcd 26.75) for C, 2.52 (calcd 2.24) for H, and 6.40 (calcd 6.24) for N.

$(ZnSO_3)_2$(2,2′-bipy)H_2O (2). Zinc carbonate (0.1582 g), ammonium sulfite monohydrate (0.1725 g), 2,2′-bipyridine (0.1543 g), methanesulfonic acid (99.5%, 0.1915 g, used for the adjustment of pH), ethylene glycol (1.7002 g), and distilled water (6.2176 g) were mixed in a 23 mL Teflon cup, and the mixture was stirred for 20 min. The pH value was 5.43. The vessel was then sealed and heated at 120 °C for 7 d. The autoclave was subsequently allowed to cool to room temperature. The plate-shaped transparent colorless crystals were obtained in 56% yield. Results of elemental analysis (in wt %) for **2**, $C_{10}H_{10}N_2O_7S_2Zn_2$, are 25.98 (calcd 25.83) for C, 2.39 (calcd 2.17) for H, and 5.80 (calcd 6.02) for N.

$(ZnSO_3)_2$(TMDPy) (3). Zinc carbonate (0.1267 g), potassium sulfite (0.2058 g), 4,4′-trimethylenedipyridine (0.3000 g), acetic acid (0.1401 g, used for the adjustment of pH), ethylene glycol (2.0223 g), and distilled water (6.2188 g) were mixed in a 23 mL Teflon cup, and the mixture was stirred for 20 min. The pH value was 6.13. The vessel was then sealed and heated at 120 °C for 7 d. The autoclave was subsequently allowed to cool to room temperature. The plate-shaped transparent colorless crystals were obtained in 67% yield. Results of elemental analysis (in wt %) for **3**, $C_{13}H_{13}N_2O_6S_2Zn_2$, are 32.15 (calcd 31.99) for C, 2.60 (calcd 2.68) for H, and 5.49 (calcd 5.74) for N.

$(MnSO_3)_2$en (4). Manganese nitrate hydrate (98%, 0.277 g), ammonium sulfite monohydrate (0.408 g), and 6 g of water were mixed in a vial for 10 min. Then, ethylenediamine (0.100 g) was added to the above mixture and stirred for another 10 min. The pH of the resulting mixture was 9.40. The vessel was sealed and heated at 110 °C for 4 days. After cooling to room temperature, clear orange-brown needle-shaped crystals were obtained in 45% yield. Results of elemental analysis (in wt %) for **4**, CH_4NO_3SMn, are 6.85 (calcd 7.28) for C, 2.12 (calcd 2.44) for H, and 8.61 (calcd 8.49) for N.

(7) (a) Lin, Z.; Zhang, J.; Zheng, S.; Yang, G.-Y. *Solid State Sci.* **2004**, *6*, 371. (b) Lin, Z.; Zhang, J.; Zheng, S.-T.; Yang, G.-Y. *Eur. J. Inorg. Chem.* **2004**, 953. (c) Zhong, Y.-J.; Chen, Y.-M.; Sun, Y.-Q.; Yang, G.-Y, *J. Solid State Chem.* **2005**, *178*, 2613−2619. (d) Zhong, Y.-J.; Chen, Y.-M.; Sun, Y.-Q.; Yang, G.-Y. *Z. Anorg. Allg. Chem.* **2005**, *631*, 1957−1960.

(8) (a) Liang, J.; Li, J.; Yu, J.; Chen, P.; Fang, Q.; Sun, F.; Xu, R. *Angew. Chem. Int. Ed.* **2006**, *45*, 1. (b) Zhang, D.; Yue, H.; Shi, Z.; Feng, S. *Solid State Sci.* **2005**, *7*, 1256.

(9) (a) Baerlocher, C.; Meier, W. M.; Olson, D. H. *Atlas of Zeolite Framework Types*; Elsevier: Amsterdam, The Netherlands, 2001. (b) Huo, Q.; Xu, R.; Li, S.; Ma, Z.; Thomas, J. M.; Jones, R. H.; Chippindale, A. M. *J. Chem. Soc., Chem. Commun.* **1992**, 875−876.

(10) (a) Gier, T. E.; Bu, X.; Wang, S.; Stucky, G. D. *J. Am. Chem. Soc.* **1996**, *118*, 3039. (b) Harrison, W. T. A.; Phillips, M. L. F.; Nenoff, T. M.; MacLean, E. J.; Teat, S. J.; Maxwell, R. S. *J. Chem. Soc., Dalton Trans.* **2001**, 546−549.

(11) (a) Rao, C. N. R.; Behera, J. N.; Dan, M. *Chem. Soc. Rev.* **2006**, *35*, 375−387. (b) Ayyappan, S.; Bu, X.; Cheetham, A. K. *Chem. Commun.* **1998**, 2181−2182.

(12) (a) Harrison, W. T. A.; Phillips, M. L. F.; Stanchfield, J.; Nenoff, T. M. *Angew. Chem. Int. Ed.* **2000**, *39*, 3808−3810. (b) Millange, F.; Serre, C.; Cabourdin, T.; Marrot, J. Ferey, G. *Solid State Sci.* **2004**, *6*, 229−233.

(13) (a) Diaz de Vivar, M. E.; Baggio, S.; Munoz, J. C.; Baggio, R. *Acta. Crystallogr.* **2005**, *C61*, m30−m33. (b) Long, D. −L.; Kogerler, P.; Cronin, L. *Angew. Chem. Int. Ed.* **2004**, *43*, 1817. (c) Manos, M. J.; Miras, H. N.; Tangoulis, V.; Woollins, J. D.; Slawin, A. M. Z.; Kabanos, T. A. *Angew. Chem. Int. Ed.* **2003**, *42*, 425. (d) Long, D. −L.; Abbas, P.; Kogerler, P.; Cronin, L. *Angew. Chem. Int. Ed.* **2005**, *44*, 3415.

(14) (a) Chen, L.; Bu, X. *Inorg. Chem.* **2006**, *45*, 4654−4660. (b) Chen, L.; Bu, X. *Chem. Mater.* **2006**, *18*, 1857−1860.

(15) (a) Nguyen, D-T.; Bu, X. *Inorg. Chem.* **2006**, *45*, 10410−10412. (b) Nguyen, D.-T.; Chew, E.; Zhang, Q.; Choi, A.; Bu, X. *Inorg. Chem.* **2006**, *45*, 10722−10727.

Table 1. Summary of Crystal Data and Refinement Results

complexes	1	2	3	4
empirical formula	$C_5H_5NO_3SZn$	$C_{10}H_{10}N_2O_7S_2Zn_2$	$C_{13}H_{13}N_2O_6S_2Zn_2$	CH_4NO_3SMn
structural formula	$(ZnSO_3)py$	$(ZnSO_3)_2(2,2'\text{-bpy})H_2O$	$(ZnSO_3)_2(TMDPy)$	$(MnSO_3)_2en$
fw	224.53	465.06	488.11	165.06
temp (K)	293	293	293	293
A (Å)	4.9404(3)	14.1016(10)	10.56520(10)	15.7400(6)
B (Å)	8.7820(5)	12.4216(8)	9.64940(10)	4.8958(2)
C (Å)	17.1114(9)	8.5128(6)	17.0340(2)	5.9311(2)
β (deg)	96.395(4)	105.538(3)	102.6820(10)	90.00
V (Å^3)	737.79(7)	1436.64(17)	1694.21(3)	457.05(3)
Z	4	4	4	4
space group	$P2_1/c$	$P2_1/c$	$P2_1/n$	$Pnnm$
$2\theta_{max}$ (deg)	42	71	48	72
total data	6395	39891	25145	11022
unique data	745 [R(int) = 0.0563]	6006 [R(int) = 0.0245]	2749 [R(int) = 0.0842]	1072[R(int) = 0.0210]
data, $I > 2\sigma(I)$	556	4713	2145	998
params	100	208	226	41
$R(F)$ ($I > 2\sigma(I)$)	0.0331	0.0261	0.0302	0.0178
$R_w(F^2)$($I > 2\sigma(I)$)	0.0760	0.0713	0.0747	0.0507
GOF	1.095	1.125	0.954	1.193

Thermal Analysis. The thermogravimetric analysis was performed on a TA Instruments SDT Q600 under a flowing nitrogen atmosphere. The flow rate of the nitrogen gas was controlled at about 100 liters per minute. A total of 5.6090 mg of **1**, 9.3120 mg of **2**, 7.3890 mg of **3**, and 29.5120 mg of **4** were heated between room temperature and 1000 °C at a heating rate of 5 °C/min.

X-ray Powder Diffraction. X-ray powder diffraction experiments were performed on a Bruker D8 Advance X-ray powder diffractometer operating at 40 kV and 40 mA (Cu Kα radiation, λ = 1.5418 Å). Data collection was carried out with a step size of 0.03 degrees and a counting time of 1 s per step. The 2-theta angular range is from 5 to 40 degrees.

Single-Crystal Structure Analysis. Each crystal was glued to a thin glass fiber with epoxy resin and mounted on a Bruker APEX II diffractometer equipped with a fine focus, 2.0 kW sealed-tube X-ray source (Mo Kα radiation, λ = 0.71073 Å) operating at 50 kV and 30 mA. The empirical absorption correction was based on equivalent reflections, and other possible effects such as absorption by the glass fiber were simultaneously corrected. Each structure was solved by direct methods followed by successive difference Fourier methods. All non-hydrogen atoms were refined anisotropically. Computations were performed using SHELX-TL, and final full-matrix refinements were against F^2. The crystallographic results are summarized in Table 1.

Results and Discussion

$(ZnSO_3)$Py (1): A Rail-Like Inorganic $ZnSO_3$ Double Chain with Pendant Organic Ligands. In compound **1**, Zn^{2+} and SO_3^{2-} form an infinite neutral rail-like double chain along the *a* axis. As shown in Figure 1, all of the Zn^{2+} ions in the $ZnSO_3$ double chain are tricoordinated to three O atoms of three different SO_3^{2-} units, and each SO_3^{2-} unit connects to three Zn^{2+} ions. Thus, both Zn^{2+} and SO_3^{2-} serve as three-connected centers. The distances between adjacent Zn−Zn centers are 3.832(1), 4.001(1), and 4.940(1) Å, respectively. Each neutral pyridine ligand binds to one Zn^{2+} ion via its N site, which completes the fourth coordination of Zn^{2+} ions (Zn−N 2.055(6) Å). Within the $ZnSO_3$ double chain, two Zn atoms and two S atoms (from two sulfite anion) form a 4-membered ring (Zn_2S_2, not counting four bridging oxygen sites). Such 4-membered rings extend in two directions to form the $ZnSO_3$ double chain through the edge-sharing of 4-ring units.

Thermal analysis shows that compound **1** is stable until approximately 180 °C, which is the onset temperature for a gradual weight loss of 65.6% between 180 and 800 °C. Because the weight percentage of the organic component is only 35.23%, the loss of pyridine is also accompanied by the loss of SO_2 (calcd 28.51%). The total experimental weight loss is about 1% lower than the calculated value of 36.3% for the decomposition of $(ZnSO_3)$Py into ZnO.

$(ZnSO_3)_2(2,2'\text{-bipy})H_2O$ (2): An Inorganic Double Chain from Alternating 3- and 4-Membered Rings. In compound **2**, Zn^{2+} ions are also bridged by SO_3^{2-} anions to form an infinite neutral double chain along the *c* axis. However, the bonding pattern in compound 2 is dramatically different from that in compound **1**, illustrating the structural diversity that can be achieved in the $Zn-SO_3^{2-}$ system. As shown in Figure 2, there are two independent Zn^{2+} ions with different coordination geometry. Zn1 is tetrahedrally coor-

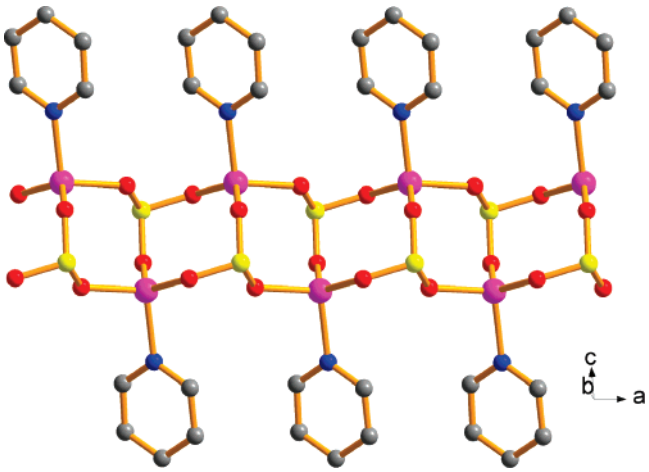

Figure 1. Rail-like chain in complex **1**. Purple, Zn; Yellow, S; Red, O; Blue, N; Gray, C.

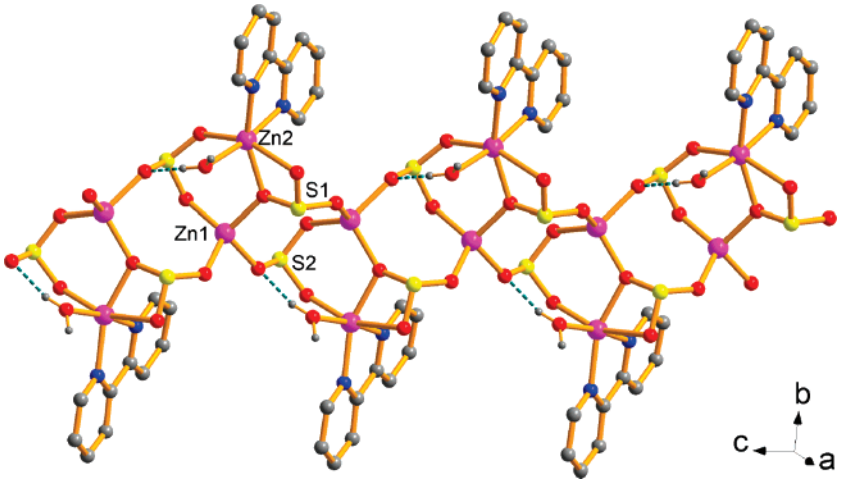

Figure 2. Double chain in complex **2**. Hydrogen bonds were shown as dashed lines. Purple, Zn; Yellow, S; Red, O; Blue, N; Gray, C.

dinated by four O atoms coming from four different SO_3^{2-} anions. In contrast, Zn2 has distorted octahedral coordination geometry and is bonded by three O atoms coming from only two different SO_3^{2-} anions. The three remaining coordination bonds of Zn2 are made to one aqua O atom and two N atoms of the same 2,2′-bipy ligand. It is worth noting that Zn1 and Zn2 share one common oxygen site from a SO_3^{2-} group.

The structural complexity of compound **2** is further increased by the occurrence of two independent and coordinatively different SO_3^{2-} anions. Whereas both of them use all three O atoms to connect to three Zn^{2+} ions, their bonding modes are not the same. One SO_3^{2-} group (S2) is connected to three Zn^{2+} sites with all of the oxygen sites bicoordinated between the Zn^{2+} and S^{4+} sites, similar to the bonding pattern in compound **1**. On the other hand, in the other SO_3^{2-} group (S1), one oxygen site is tricoordinated between two Zn^{2+} sites and one S^{4+} site. The Zn−O−Zn linkage allows the formation of the 3-membered ring (Zn1, Zn2, and S2, with three bridging oxygen sites not counted). The 4-membered ring is formed between two crystallographically identical Zn1 sites, one S1 site, and one S2 site. These 3- and 4-membered rings alternate to form a wavy double chain.

The 2,2′-bipy ligands chelate the Zn2 sites and are located at two sides of the double chain with molecular planes parallel to one another. Along the same side, the distance between the two adjacent 2,2′-bipy ligands is 8.513 Å. The gap is so wide that the 2,2′-bipy ligand from the adjacent chain partially fills the gap, as shown in Figure 3. Weak $\pi-\pi$ interactions are found between two pyridine rings of two 2,2′-bipy ligands with a center-to-center distance of 3.638 Å. Such $\pi-\pi$ interactions result in the formation of a layer parallel to the *bc* plane.

It is interesting to note that the aqua ligand forms two types of hydrogen bonds. One is the intrachain hydrogen bond (O1W···O6 = 2.7919(19) Å), and another is the interchain hydrogen bond (O1W···O2^i = 2.7892(17) Å; symmetry code: $i = -x+1, -y+1, -z+1$). Two adjacent layers are linked face-to-face by interchain hydrogen bonds, forming a double-layer structure (Figure 4). The further

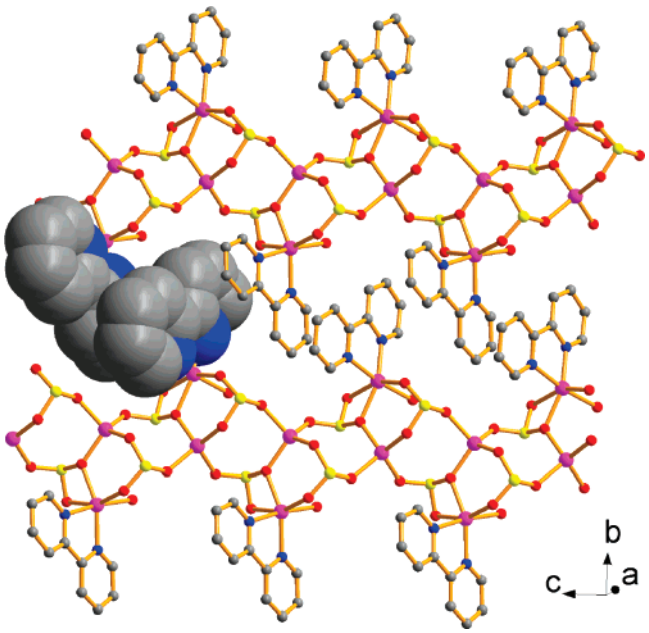

Figure 3. Space-filling view of two 2,2′-bipy ligands and the $\pi-\pi$ interactions in complex **2**. Purple, Zn; Yellow, S; Red, O; Blue, N; Gray, C.

stacking of such double layers leads to the observed crystal structure. The interactions between double layers are assumed to be van der Waals forces.

Thermal analysis of compound **2** shows two steps of weight losses. The first weight loss occurs between 50 and 200 °C with an observed weight loss of 3.46% corresponding to the loss of the water molecules (calcd 3.87%). The second weight loss of 63.04% occurs in the range of 225−945 °C, which can be attributed to the elimination of 2,2′-bipy (calcd 33.55%) and SO_2 (calcd 27.53%). The remaining weight of 33.5% is likely that of ZnO (calcd 35.06%).

$(ZnSO_3)_2$(TMDPy) (3): From 1D Inorganic Chain to 2D Inorganic−Organic Hybrid Layers. Compound **3** also contains inorganic $ZnSO_3$ chains, but it is very different from chains in compounds **1** and **2**. As shown in Figure 5, two independent Zn^{2+} ions (Zn1 and Zn2) and two independent SO_3^{2-} anions alternate to form an infinite chain along the *b* direction. Two independent SO_3^{2-} anions have the same

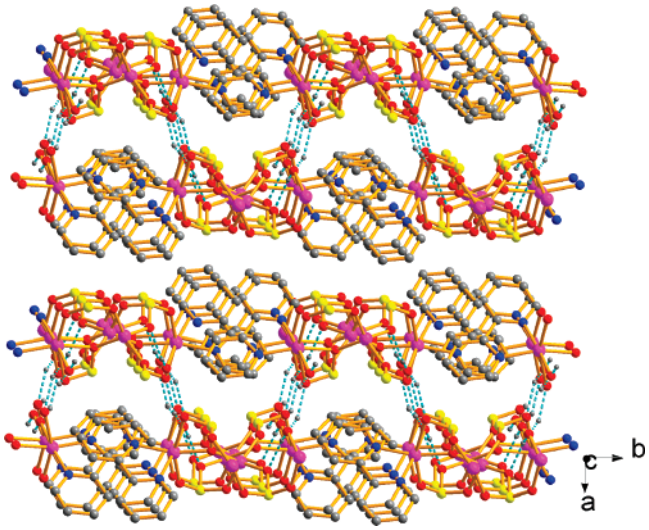

Figure 4. 3D stacking structure of complex **2**. Hydrogen bonds were shown as dashed lines. Purple, Zn; Yellow, S; Red, O; Blue, N; Gray, C.

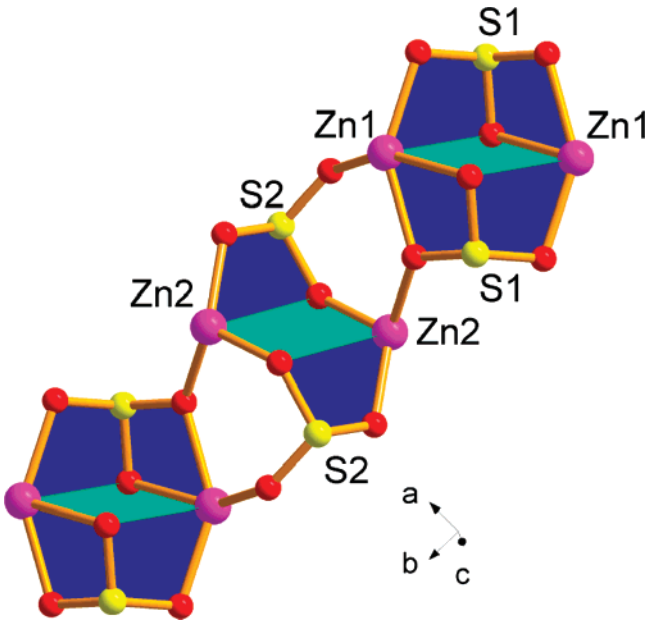

Figure 5. View of a chain containing two types of chairlike dimeric units in complex **3**. Purple, Zn; Yellow, S; Red, O.

coordination mode as that in the complex **2**, and both of them use all three O atoms to connect to three Zn^{2+} ions. On the other hand, the bonding modes of two Zn^{2+} sites differ from those observed in compounds **1** and **2**. Two Zn^{2+} ions have tetrahedral (Zn2) and distorted square-pyramidal geometries (Zn1), respectively.

Two symmetry-related SO_3^{2-} anions (S1) coordinate to two Zn1 centers with a Zn−Zn distance of 3.610 Å, which leads to the formation of a chairlike dimeric unit. In comparison, two symmetry-related SO_3^{2-} anions (S2) bridge two Zn2 centers, which also lead to the formation of a chairlike dimeric unit, distinctly different from the dimeric unit formed by Zn1 and S1 sites. The Zn−Zn distance within the second type of dimer is slightly shorter (3.489 Å). These two types of chairlike dimeric units are linked through a 3-ring unit (−S2−O−Zn1−O−Zn2−O) into an infinite inorganic chain (Figure 5).

Each Zn site has an available bond for connection with the organic ligand, and each TMDPy ligand joins together two independent Zn sites (Zn1 and Zn2) of two adjacent chains through the Zn−N bond (Zn1−N2 = 2.052(2) and Zn2−N1 = 2.024(2) Å). The distance between two TMDPy-connected Zn sites is 13.953 Å. A 2D sheet that is parallel to the *ab* plane is formed (Figure 6).

Thermal analysis shows that compound **3** is stable until approximately 220 °C, which is the onset temperature for a gradual weight loss of 66.9% between 250 and 975 °C. Because the weight percentage of the organic component is only 40.57%, the loss of TMDPy is also accompanied by the loss of SO_2 (calcd 26.23%). The total experimental weight loss is about 0.3% lower than the calculated value of 33.4% for the decomposition of $(ZnSO_3)_2$(TMDPy) into ZnO.

$(MnSO_3)_2$en (4): A 3D Framework by Pillaring Helix-Containing Layers. In compound **4**, Mn^{2+} and SO_3^{2-} form infinite neutral 2D layers that are crosslinked into a 3D framework by ethylenediamine molecules through Mn−N bonds. Within the $MnSO_3$ layer, Mn^{2+} and O^{2-} (from the sulfite anion) form an approximately square grid-type structure (Mn_4O_4) (Figure 7). Each Mn^{2+} is bonded to five oxygen atoms of four separate SO_3^{2-} groups (two oxygen sites from a single SO_3^{2-} group and three other oxygen sites from three separate SO_3^{2-} groups). Each SO_3^{2-} group is in turn connected to four Mn^{2+} sites with one oxygen site bicoordinated between one Mn^{2+} and one S^{4+} site and two oxygen sites tricoordinated between two Mn^{2+} and one S^{4+} sites. In other words, two oxygen atoms of the SO_3^{2-} anion form a bridging mode across two Mn^{2+} sites with an Mn−Mn distance of 3.896 Å. Such tricoordinated O atoms link Mn^{2+} sites to form left- and right-handed helices along the *b* axis. The left- and right-handed helices are not intertwined together. Instead, they are arranged side-by-side along the *c* direction.

Within the $MnSO_3$ layer, the S^{4+} site and two tricoordinated O atoms of the SO_3^{2-} anion behave as 3-connected nodes, and the Mn^{2+} sites act as 5-connected nodes. The layer can be topologically represented as a 2D (3,5)-connected plane. The coordination environment of each Mn^{2+} site is completed by the N atoms of the ethylenediamine ligand and exhibits distorted octahedral geometry. Ethylenediamine molecules on two adjacent Mn^{2+} sites are distributed on opposite sides of the layer (Figure 8), which serves to cross-link adjacent neutral $MnSO_3$ layers into a 3D framework (Figure 9). When the bridging ethylenediamine molecules are taken into consideration, each Mn^{2+} site becomes 6-connected, and the whole framework is thus a 3D (3,6)-connected net.

Thermal analysis shows that compound **4** is stable until approximately 200 °C, which is the onset temperature for a gradual weight loss of 52.9% between 200 and 690 °C. Because the weight percentage of the organic component is only 18.45%, the loss of ethylenediamine is also accompanied by the loss of SO_2 (calcd 38.81%). The total experimental weight loss is about 4% lower than the calculated value of 57.3% for the decomposition of $(MnSO_3)_2$-en into MnO.

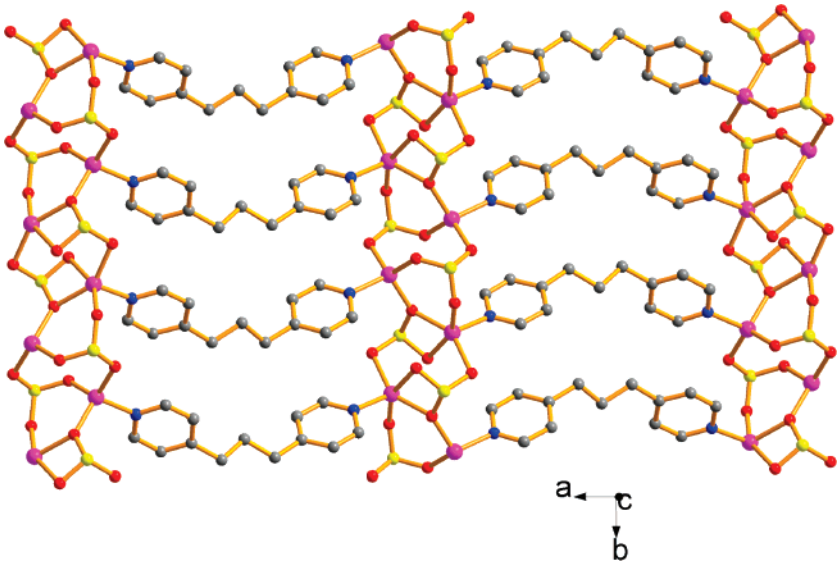

Figure 6. 2D layer in complex **3** viewed down the *c* axis. Purple, Zn; Yellow, S; Red, O; Blue, N; Gray, C.

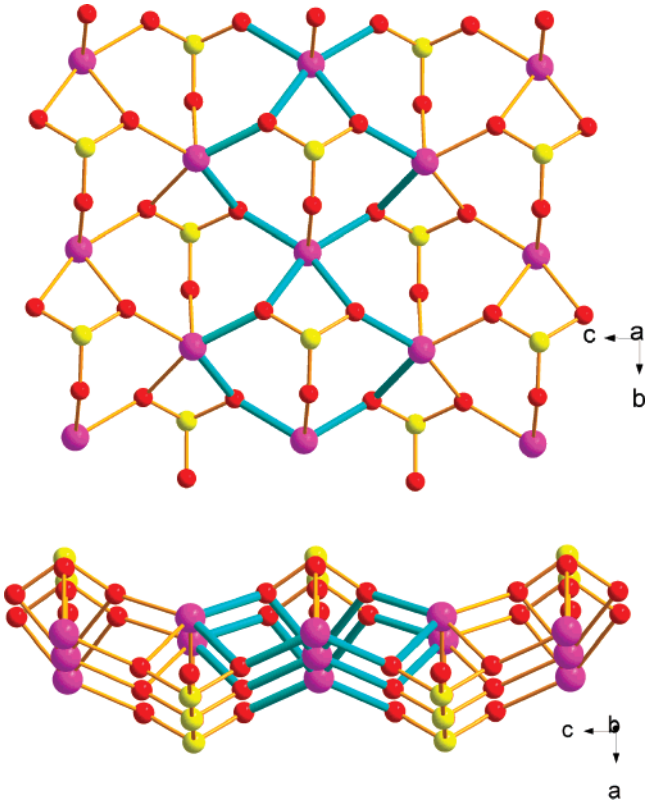

Figure 7. Top, the infinite $MnSO_3$ layer in complex **4** viewed down the *a* axis; bottom, the layer viewed down the *b* axis, showing left and right helices. Purple, Mn; Yellow, S; Red, O.

The magnetic susceptibility of **4** was measured in the range 2−300 K at 5000 Oe (Figure 10). The $\chi_m T$ value of each Mn unit (4.45 cm^3 K mol^{-1}) at 300 K is almost equal to that (4.37 cm^3 K mol^{-1}) expected for one magnetically isolated high-spin Mn(II) ion. Upon cooling, $\chi_m T$ decreases smoothly to a minimum (1.99 cm^3 K mol^{-1}) at 22 K, indicating the presence of a dominant antiferromagnetic interaction. Then, it increases rapidly as the temperature decreases to 13 K ($\chi_m T$ value = 2.71 cm^3 K mol^{-1}). These features are indicative of ferrimagnetic behavior. The decrease of $\chi_m T$ below 13 K results from a saturation of the χ_m value and/or the zero-field splitting effect. Because the $Mn(SO_3)$ layers in **4** are well separated by the en bridges, the ferrimagnetic behavior can be suggested to arise from intralayer magnetic interactions. The magnetic susceptibility above 22 K obeys the Curie−Weiss law ($1/\chi_m = (T-\Theta)/C$) with the Curie constant, *C*, of 4.93 cm^3 K mol^{-1} and a negative Weiss constant, Θ, of −34.86 K, which also indicates an intralayer antiferromagnetic coupling between the adjacent Mn(II) ions through the SO_3 bridges.

Structural Variations, Comparisons, and Trends. From the above structural descriptions, it is clear that metal ions and SO_3^{2-} anions can form unique inorganic subunits that can be chains or layers. The large structural variations are closely associated with the flexible coordination chemistry of SO_3^{2-} and metal cations. Within these structures, the oxygen atoms in the SO_3^{2-} anion exhibit two types of bonding modes: (I) the bicoordination mode between one metal site and one sulfur site as in **1**, **2**, **3**, and **4**; and (II) the tricoordination mode between two metal sites and one sulfur site as in **2**, **3**, and **4**. Such bonding modes have been observed before in other sulfites such as $[Zn_2(SO_3)_2(C_{12}H_{12}N_2)(H_2O)]_n$ and $[Zn_2(SO_3)_2(C_{12}H_{12}N_2)_2]\cdot 2H_2O$.[13] Bonding mode II is much less common in phosphites, which accounts for the observed structural differences between these sulfites and similarly prepared phosphites.

The four polymeric materials possess combinations of bonding types I and II in different ratios. In compound **1**, only type I is observed (I to II ratio = 100:0), whereas in compounds **2** and **3**, only one oxygen site on the S1 site is type II, and five other oxygen sites (two on the S1, three on S2) are type I (I to II ratio = 83.3:16.7). In contrast, compound **4** has a much higher percentage of the type II mode, with two oxygen sites being type II and only one oxygen site being type I (I to II ratio = 33.3:66.7). Thus,

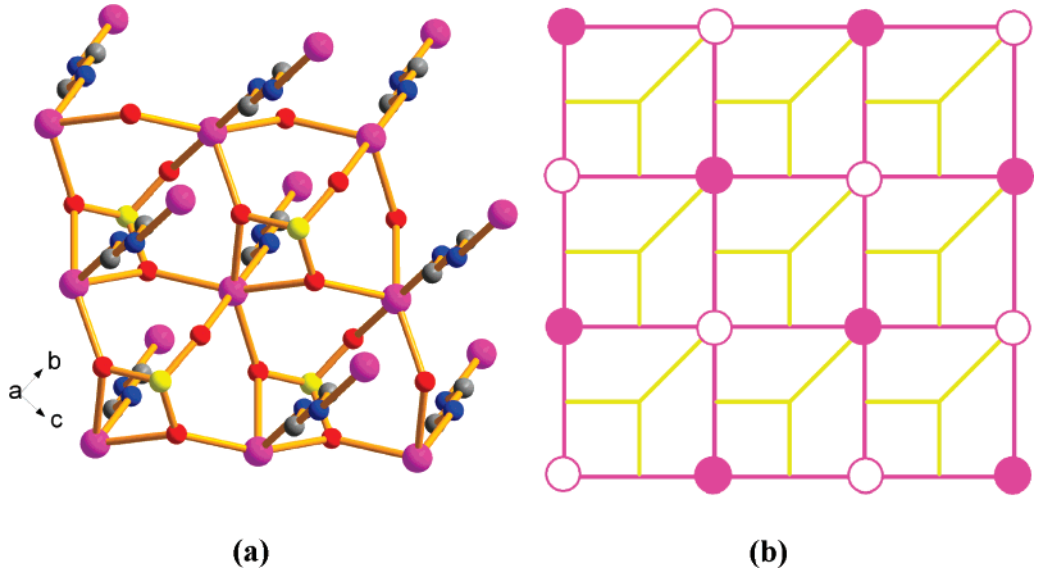

Figure 8. (a) Ethylenediamine ligands are located at two sides of the layer. (b) The schematic representation of the (3,5)-connected plane in complex **4**; solid circles and open circles represent two different bonding directions of the ethylenediamine ligands.

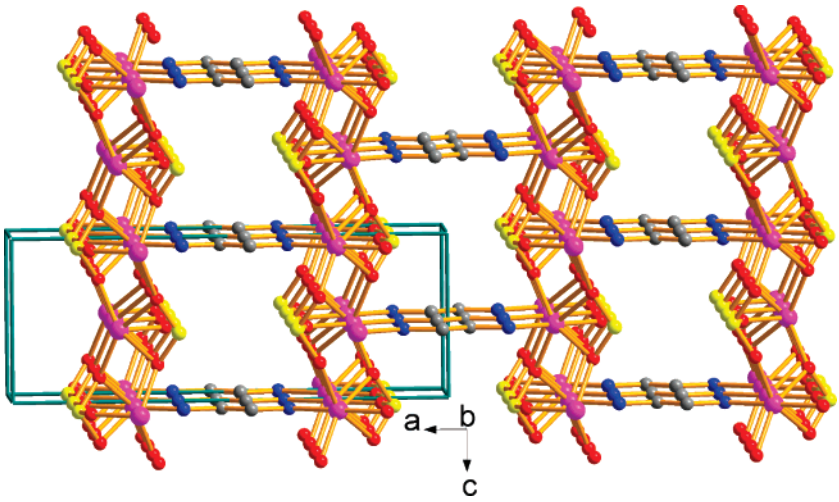

Figure 9. Viewed down the *b* axis, the infinite $MnSO_3$ sheets are pillared by neutral ethylenediamine molecules into a 3D open framework in $(MnSO_3)_2$en. Purple, Mn; Yellow, S; Red, O; Blue, N; Gray, C.

there is a progressive increase in the type II bonding mode from **1** to **4**.

Another structural feature in these sulfites is the chelating bonding mode, which is rarely found in phosphites. In compounds **2** and **3**, two oxygen sites (types I and II) of the same sulfite group bind to the same metal site. In comparison, in compound **4**, two oxygen sites (both type II) of the same sulfite group bind to the same metal site.

Parallel to the coordination variations of SO_3^{2-}, the metal site in these polymeric structures also displays different coordination geometry. In compound **1**, all of the metal sites (Zn^{2+}) are tetrahedrally coordinated, whereas in compound **2**, octahedrally coordinated Zn^{2+} sites coexist with tetrahedrally coordinated Zn^{2+} sites. Compound **3** has a unique combination between pentacoordinated Zn^{2+} sites and tetrahedrally coordinated Zn^{2+} sites. All of the metal sites (Mn^{2+}) in compound **4** are octahedrally bonded because of the stronger preference for the octahedral coordination by Mn^{2+}.

The interplay of these coordination features of metal sites and SO_3^{2-} results in neutral inorganic units with alternating metal sites and SO_3^{2-} anions. Such inorganic subunits of different dimensionality (1D and 2D) are subsequently connected into extended frameworks of higher dimensionality (2D and 3D) by using bifunctional organic ligands, as in compounds **3** and **4**. In comparison, metal phosphites are more likely to form negatively charged polymeric units from 1D to 3D with protonated amine molecules as extraframework charge-balancing species. So far, no 2D or 3D metal−sulfite frameworks that encapsulate protonated organic amines have been prepared, which highlights the different crystal chemistry between sulfites and phosphites.

Conclusion

This work reports four new inorganic−organic hybrid structures based on metal−sulfite chains and layers. The tendency of the metal−sulfite system to form polymeric inorganic units is different from commonly observed metal−

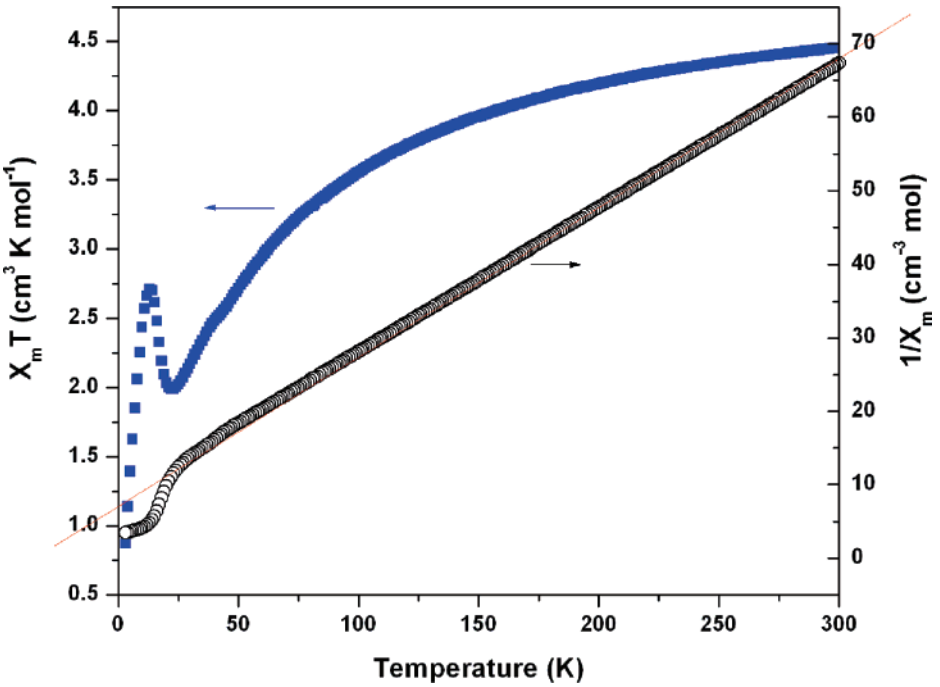

Figure 10. $1/\chi_m$ and $\chi_m T$ versus T plot with the theoretical fit (-) for compound **4**.

organic frameworks that are dominated by structures with isolated inorganic and organic units. Because of the occurrence of the polymeric inorganic unit, the metal−sulfite system illustrated here has the potential to help develop framework materials with unique physical properties such as low-dimensional magnetism and electronic properties that are characteristic of inorganic materials. It is clear from the results reported here that the inorganic−organic hybrid metal−sulfite system is very unique, and its crystal chemistry cannot be extrapolated from earlier studies of other related systems such as metal phosphites. Its potential to be used in the construction of crystalline open-framework materials awaits further synthetic and structural exploration.

Acknowledgment. We thank the support of this work by NIH (X.B., Grant 2 S06 GM063119-05), NSF-MRI (Y.Y.G. and X.B.), the NIH-RISE program (X.B.), Research Corporation (X.B., Grant CC6593), the donors of the Petroleum Research Fund (administered by the ACS) (X.B., Grant 41382-GB10), and the National Science Foundation (P.F.).

Supporting Information Available: Crystallographic data including positional parameters, thermal parameters, bond distances and angles (CIF), ORTEP diagrams, experimental and simulated X-ray powder patterns, and TGA plots for compounds **1**−**4**. This material is available free of charge via the Internet at http://pubs.acs.org.

IC070325H